Atmos. Meas. Tech., 8, 1593–1604, 2015
www.atmos-meas-tech.net/8/1593/2015/
doi:10.5194/amt-8-1593-2015

Atmospheric Measurement Techniques
Open Access

The impact of the microphysical properties of aerosol on the atmospheric correction of hyperspectral data in coastal waters

C. Bassani[1], C. Manzo[1], F. Braga[2], M. Bresciani[3], C. Giardino[3], and L. Alberotanza[2]

[1]Institute for Atmospheric Pollution Research (IIA), Italian National Research Council (CNR), Via Research Area of Rome 1, Via Salaria Km 29 300, 00016 Monterotondo Scalo, Rome, Italy
[2]Institute of Marine Sciences (ISMAR), Italian National Research Council (CNR), Arsenale Tesa 104, Castello 2737/F, 30122 Venice, Italy
[3]Institute for Electromagnetic Sensing of the Environment (IREA), Italian National Research Council (CNR), Via Bassini 13, 20133 Milan, Italy

Correspondence to: C. Bassani (cristiana.bassani@iia.cnr.it)

Received: 6 February 2014 – Published in Atmos. Meas. Tech. Discuss.: 23 May 2014
Revised: 6 March 2015 – Accepted: 13 March 2015 – Published: 27 March 2015

Abstract. Hyperspectral imaging provides quantitative remote sensing of ocean colour by the high spectral resolution of the water features. The HICO™ (Hyperspectral Imager for the Coastal Ocean) is suitable for coastal studies and monitoring. The accurate retrieval of hyperspectral water-leaving reflectance from HICO™ data is still a challenge. The aim of this work is to retrieve the water-leaving reflectance from HICO™ data with a physically based algorithm, using the local microphysical properties of the aerosol in order to overcome the limitations of the standard aerosol types commonly used in atmospheric correction processing. The water-leaving reflectance was obtained using the HICO@CRI (HICO ATmospherically Corrected Reflectance Imagery) atmospheric correction algorithm by adapting the vector version of the Second Simulation of a Satellite Signal in the Solar Spectrum (6SV) radiative transfer code. The HICO@CRI algorithm was applied on to six HICO™ images acquired in the northern Mediterranean basin, using the microphysical properties measured by the Acqua Alta Oceanographic Tower (AAOT) AERONET site. The HICO@CRI results obtained with AERONET products were validated with in situ measurements showing an accuracy expressed by $r^2 = 0.98$. Additional runs of HICO@CRI on the six images were performed using maritime, continental and urban standard aerosol types to perform the accuracy assessment when standard aerosol types implemented in 6SV are used. The results highlight that the microphysical properties of the aerosol improve the accuracy of the atmospheric correction compared to standard aerosol types. The normalized root mean square (NRMSE) and the similar spectral value (SSV) of the water-leaving reflectance show reduced accuracy in atmospheric correction results when there is an increase in aerosol loading. This is mainly when the standard aerosol type used is characterized with different optical properties compared to the local aerosol. The results suggest that if a water quality analysis is needed the microphysical properties of the aerosol need to be taken into consideration in the atmospheric correction of hyperspectral data over coastal environments, because aerosols influence the accuracy of the retrieved water-leaving reflectance.

1 Introduction

Hyperspectral imaging is well suited to investigating water quality in coastal environments where a local scale is required in the case of optically complex coastal waters (Amin et al., 2014; Gitelson et al., 2011; Gao et al., 2009). For these applications, the water-leaving reflectance has to be obtained by accurate atmospheric modelling because only 10 % of the total radiance received by sensor come from the water target (Antoine and Morel, 1999).

In this context, many authors (IOCCG, 2010; Gao et al., 2000) demonstrated the crucial role of the aerosol in atmospheric radiative transfer modelling and, consequently, on the

accuracy of the results of mainly large-scale atmospheric correction of multi- and hyperspectral remote sensing data.

A series of physically based algorithms to retrieve aerosol properties and water-leaving reflectance from remote sensing images have been developed, using MODIS (Tanré et al., 1997; Gordon and Wang, 1994), SeaWIFS (Gordon and Wang, 1994) and MERIS (Antoine and Morel, 1999). Retrieving the water-leaving reflectance involves the removal of the sea surface contribution due to sun, view geometry and wind speed (McClain, 2009; Morel and Gentili, 1996, 1991; Gordon and Wang, 1992) in addition to removing the atmospheric contribution from the total sensor signal.

IOCCG (2010) provides a detailed description of the algorithms for atmospheric correction over water. The described atmospheric correction algorithms perform well in clear ocean waters, whereas they can induce errors if applied in turbid waters (Mélin et al., 2007; Zibordi et al., 2006). Significant errors were also obtained when software dedicated to the atmospheric correction of hyperspectral data (i.e. ATREM) was applied to coastal water (Amin et al., 2014; Gitelson et al., 2011).

Regarding the aerosol type during the atmospheric correction of remote sensing data, Gordon and Wang (1994) highlighted that standard aerosol types are a simplification of the actual microphysical properties of the aerosol at the acquisition time. To overcome this limitation, a new set of aerosol models has been introduced to improve the description of aerosol properties in the coastal environment (Ahmad et al., 2010). Zibordi et al. (2009a) proved the effects of a limited number of aerosol types on the ocean colour primary products in this coastal region, confirming that the local aerosol, described by specific microphysical properties, might not be represented by standard aerosol types in coastal environments.

The focus of this work is to analyze the impact of the microphysical properties of the aerosol on the results of the atmospheric correction of the HICO™ (Hyperspectral Imager for the Coastal Ocean) data. These data are characterized by higher spatial and spectral resolution compared to the multispectral sensors commonly used for coastal environment analysis in the northern Adriatic Sea (Jamet et al., 2011; Mélin et al., 2007).

This paper is organized as follow. Section 2 describes the site and Sect. 3 reports the data used in the analysis. The new algorithm, HICO@CRI (HICO™ ATmospherically Corrected Reflectance Imagery), developed to perform the atmospheric correction of HICO™ data is explained in Sect. 4. The HICO@CRI is based on the vector version of the Second Simulation of a Satellite Signal in the Solar spectrum (6SV) atmospheric radiative transfer code (Vermote et al., 2006), which is the improved open-source code of the 6S (Vermote et al., 1997b). The water-leaving reflectance was obtained by running the HICO@CRI algorithm with the microphysical properties of the aerosol provided by the Acqua Alta Oceanographic Tower (AAOT) station (Mélin et al., 2006) of the AERONET network (Holben et al., 1998). Section 5.1 reports the validation of the results of HICO@CRI with in situ measurements acquired during oceanographic campaigns carried out at the HICO™ overpass. In Sect. 5.2, additional runs were performed with maritime, continental, and urban aerosol standard types provided by default by 6SV. Results from the first run enabled a reference to be built, against which the output obtained by running HICO@CRI with the three 6SV standard aerosol types could be compared. The NRMSE (normalized root mean square) and the similar spectral value (SSV) were used to assess the accuracy of water-leaving reflectance retrieved by atmospheric correction of hyperspectral data in coastal water when aerosol standard types are used instead of locally observed aerosol.

2 Site

The northern Adriatic Sea is the north-easternmost of the Mediterranean Sea (Fig. 1). It is a shallow basin with bottom depths not exceeding 100 m. Its oceanographic conditions are strongly influenced by the dominant winds: the Bora, a northeasterly cold and dry wind and the southeasterly humid Sirocco. The discharge of several Italians rivers (Po, Adige, Piave, etc.) is also important both in terms of buoyancy and nutrients input.

The Acqua Alta Oceanographic Tower (AAOT), shown in Fig. 1, is located in the north of the Adriatic Sea, 15 km off the Venice lagoon (12.51° E, 45.31° N). The AAOT is used to continuously collect atmosphere (wind speed and direction, air temperature, air humidity, barometric pressure, and incident solar radiation), water (in situ temperature, salinity, and sea surface height), and wave parameters. The AAOT (Mélin et al., 2006) is an automated station of the AERONET network (Holben et al., 1998) equipped with the CIMEL sun–sky radiometer instrument. Besides atmospheric acquisitions, the CIMEL at AAOT also performs ocean color measurements for the AERONET-OC network (Zibordi et al., 2009b).

The time series collected at the AAOT site seems an excellent indicator of the aerosol type over the north Adriatic Sea as well as over the northern part of the Mediterranean basin, as indicated by Mélin et al. (2006). The associated aerosol type clearly reflects dominating continental and anthropogenic influences for these regions (Mélin et al., 2006; Zibordi et al., 2006). However, the presence of maritime aerosol was also taken into account since it is located in the Mediterranean Sea.

3 Data

The remotely sensed data used in this study were acquired using two passive remote sensing instruments operating in the visible spectral domain. The atmospheric data were obtained from the in situ automatic tracking sun–sky radiometer CIMEL CE-318 of the AAOT station (Smirnov et al., 2011;

Figure 1. The study area with the location of the Acqua Alta Oceanographic Tower (AAOT) and portion of Adriatic Sea imaged by HICO™.

Mélin et al., 2006; Holben et al., 1998), while image data came from the HICO™ hyperspectral sensor (Lucke et al., 2011).

The CIMEL CE-318 provides the optical thickness of the aerosol at the nominal wavelengths (440, 500, 670, 870, 940, 1020 nm), the columnar content of water vapour, wvcc, and ozone, occ, by measuring the direct component of the solar irradiance. From the measurements of the diffuse component on four bands (442, 668, 870, 1020 nm) of the sky radiance at specific angles, the AERONET inversion products (i.e. aerosol microphysical and optical properties) are retrieved.

The atmospheric data have three quality levels: level 1.0 (unscreened), level 1.5 (cloud-screened), and level 2.0 (cloud-screened and quality-assured). Level 2.0 of atmospheric properties is used for atmospheric correction, and level 1.5 has been largely used for remote sensing applications, the microphysical properties often being limited to level 1.5.

The HICO™ sensor, (Lucke et al., 2011), is the first spaceborne hyperspectral sensor dedicated to coastal and inland monitoring and ocean characterization. The sensor is composed of 87 contiguous channels in the spectral domain 400–900 nm with the full width at half maximum (FWHM) of about 10 nm. The ground swath is about 43.5 km with a pixel size of 87 m at nadir acquisition. The vicarious calibration techniques used operationally to convert HICO digital numbers (DNs) to radiometrically calibrated radiances are described in Gao et al. (2012). The signal-to-noise ratio (SNR) is $> 200:1$ over 400–600 nm as reported in Lucke et al. (2011).

Table 1 shows the six HICO™ images with corresponding AERONET direct products provided by AAOT station, the τ_{550}, wvcc, and occ. The Ångström coefficient is also reported for the qualitative evaluation of the aerosol size from the measurements of direct solar irradiance.

Figure 2 shows the microphysical properties, size distribution, and the real and imaginary part of the refractive index retrieved from the diffuse measurements of solar radiance using the CIMEL CE-318 (AERONET inversion products provided by AAOT station). In Fig. 2a, the bimodal distribution of the aerosol size is in agreement with the results reported in Mélin et al. (2006), except for 25 April 2013 where the coarse mode prevails in the volume size distribution. The size distribution on 4 May 2011 presents a tri-modal size distribution, observed for low aerosol loading in the site (Mélin et al., 2006). The Fig. 2b and c show the real and imaginary parts of the refractive index, respectively. The spectral values of the imaginary part reveal a non-negligible absorption of aerosol in the coastal area during data acquisition, especially

Table 1. The simultaneous HICO™ and CIMEL acquisition with the τ_{550}, wvcc, occ and the Ångström coefficient downloaded from the AAOT AERONET station. The selected images meet the clear-sky requirement.

Date (yyyy/mm/dd)	HICO™ (hh:mm)	CIMEL (hh:mm)	τ_{550}	Water Vapour (cm)	Ozone (Dobson)	Ångström $\alpha_{470/870}$
2011/05/04	13:07	13:06	0.08 (lev2.0)	0.696 (lev2.0)	367.51 (lev2.0)	1.884 (lev2.0)
2012/01/11	13:21	13:18	0.05 (lev2.0)	0.949 (lev2.0)	326.23 (lev2.0)	1.769 (lev2.0)
2012/03/09	13:42	13:36	0.10 (lev2.0)	0.762 (lev2.0)	362.16 (lev2.0)	1.820 (lev2.0)
2012/05/12	07:18	07:20	0.25 (lev2.0)	2.381 (lev2.0)	364.15 (lev2.0)	1.599 (lev2.0)
2012/08/27	12:57	13:01	0.01 (lev2.0)	1.528 (lev2.0)	309.84 (lev2.0)	0.336 (lev2.0)
2013/04/25	13:03	13:08	0.27 (lev1.5)	1.969 (lev1.5)	371.40 (lev1.5)	0.851 (lev2.0)

on 11 January 2012, while observations on 4 May 2011 underlines the presence of non-absorbing particles in the atmosphere. The microphysical properties, size distribution and refractive index, mean that we can get a detailed evaluation of the aerosols' radiative impact on the atmospheric correction of hyperspectral HICO™ data. This is achieved by a more accurate modelling of the spectral behaviour of the local optical properties compared to the aerosol standard types. The aerosol optical properties required for radiative modelling and used for the atmospheric correction, were derived from these microphysical properties (Fig. 2) using the subroutines MIE and AEROSOL included in the 6SV source code (Vermote et al., 2006).

The 6SV standard aerosol types (cf. Sect. 2) are defined according to a combination of four basic components: sea-salt, water-soluble, soot and dust-like (Lenoble, 1985; d'Almeida et al., 1991; Vermote et al., 2006). Table 2 shows the volumetric percentage of the basic components for the three aerosol types. Figure 3 shows the single-scattering albedo (left) and the asymmetry parameter (right) of the three 6SV standard aerosol types and the measurement days. In Fig. 3 the continuous lines represent the optical properties simulated by the MIE and AEROSOL subroutines of 6SV, while the dots indicate the corresponding values obtained by the CIMEL measurements. Simulated and measured data are indicated with the same color for each day (cf. Table 1). Figure 3 clearly shows that the AAOT single-scattering albedo is similar to continental and maritime types, while the AAOT asymmetry parameter is more similar to the urban and continental types. From these optical properties, the local aerosol seems more similar to the continental aerosol than maritime and urban types.

Table 2. The volumetric percentage of the four basic components (sea-salt, water-soluble, soot and dust-like) describing the optical behaviour of maritime, continental, and urban aerosol types (Lenoble, 1985; d'Almeida et al., 1991; Vermote et al., 2006).

	Water-soluble	Soot	Dust-like	Oceanic
Maritime	5 %			95 %
Continental	29 %	1 %	70 %	
Urban	61 %	22 %	17 %	

In addition to AERONET data, other atmosphere and water parameters were measured at AAOT. Wind speed and direction, recorded with a VT0705B SIAP anemometer at a height of 15 m above mean sea level, were used to simulate the wind-induced water surface roughness at the time of imagery acquisitions.

In addition, two oceanographic cruises coordinated by the National Research Council of Italy (CNR), on board the *URANIA* vessel were undertaken in the study area in the second week of May 2012 and the last week of April 2013. The aim was to gather data for the calibration of a bio-optical model and the assessment of the HICO™-derived products, including water reflectance and water-quality parameters. The sampling stations (18 for 2012, 37 for 2013) included varied water types: from blue waters in the Gulf of Trieste (north-eastern Adriatic Sea) to very turbid waters at the mouths of the river deltas of the northern Adriatic Sea. The water-leaving reflectance (ρ_w) values were measured with a WISP-3 spectroradiometer (Hommersom et al., 2012) in the optical range of 380–800 nm with a spectral resolution of 1 nm. In addition two RAMSES (TriOS GmbH, Germany) sensors, RAMSES ARC VIS and RAMSES ACC

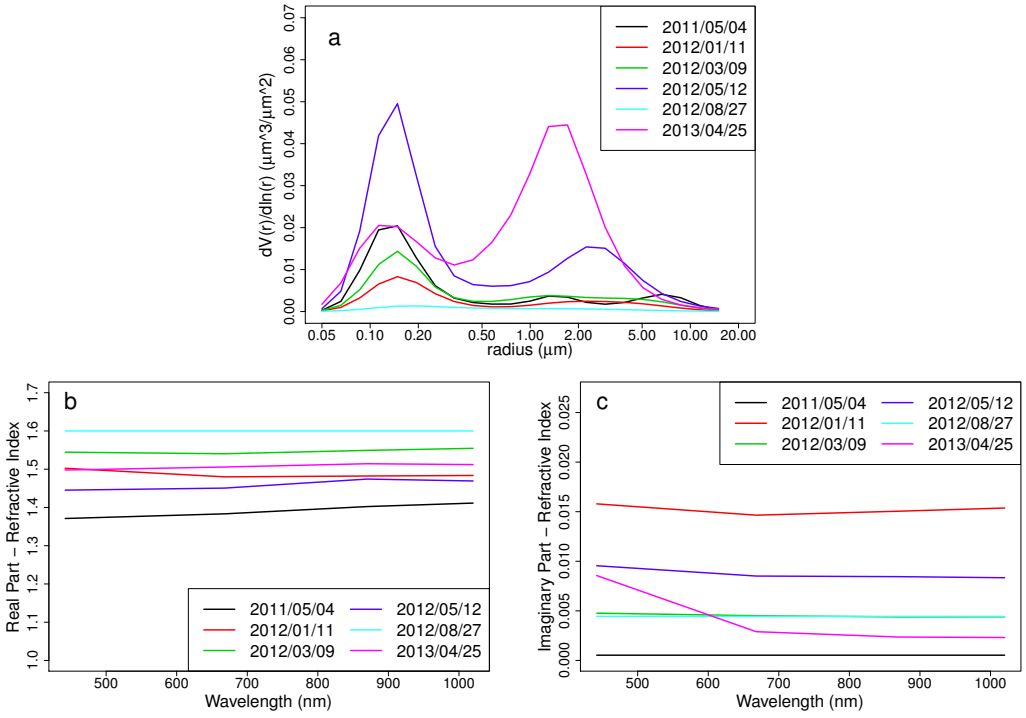

Figure 2. The microphysical properties of the aerosol downloaded from the AERONET AAOT station for the HICO™ acquisition time reported in the Table 1. The microphysical properties values are the size distribution **(a)**, the real part of the refractive index **(b)**, and the imaginary part **(c)**, of the CIMEL acquisition.

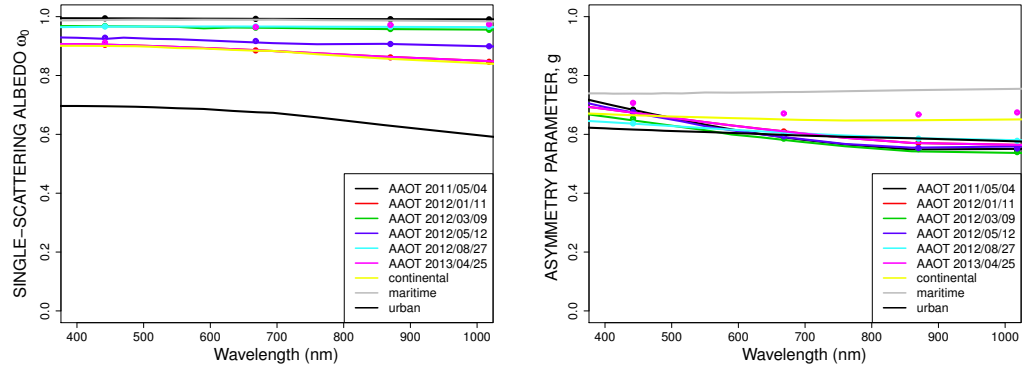

Figure 3. The single-scattering albedo and the asymmetry factor of the maritime, continental, and urban aerosol type (continuous lines) and the AERONET inversion products (dots) in the 400–900 nm spectral domain at the HICO™ acquisition time.

VIS, measured hyperspectral radiance and irradiance, respectively, both covering a wavelength range from 320 to 950 nm with one sample every 3.3 nm. A detailed description of the sampling protocols and instruments are described in Braga et al. (2013) where the location of the sites and the number of observations for each site are also provided.

4 Methods

The methodology applied in this work is based on an analysis of the contribution of aerosol microphysical properties on the accuracy of water-leaving reflectance, whose assessment is closely related to the retrieval of water quality parameters (Chlorophyll, Total Suspended Matter and Colored Dissolved Organic Matter), (Zibordi et al., 2011; Giardino et al., 2010; Guanter et al., 2010; Brando and Dekker, 2003).

The physically based algorithm, HICO@CRI, was developed for the atmospheric correction of the HICO™ image. The algorithm relies on the 6SV code, last version (Kotchenova et al., 2008) of the 6S radiative transfer code, (Vermote et al., 1997b) and was implemented in the open source GDL

programming language (Coulais et al., 2009; Arabas et al., 2010), following Bassani et al. (2010).

Starting from the at-sensor radiance, L_v, the equation presented in Vermote et al. (1997b); Vermote and Kotchenova (2008) was used under the assumption of water surface (Gao et al., 2000), for a given set of geometrical conditions according to Kotchenova and Vermote (2007). The 6SV code is thus able to simulate the crucial contributions for atmospheric correction over water, which are specular reflection, foam contribution and sun glint if present on the image (Kotchenova et al., 2006). Besides, the multiple scattering is widely identified as fundamental issue for atmospheric correction over water (IOCCG, 2010) and the 6SV provides an accurate computation of the multiple scattering contribution taking into account the effects of the aerosol types on the atmospheric radiative transfer (Vermote et al., 1997b; Kotchenova et al., 2006).

The equation solved for water-leaving radiance in reflectance units, or simply water-leaving reflectance, (Gao et al., 2000) for each HICO™ channel, ρ'_{w}, is the following:

$$\rho'_{\mathrm{w}} = \frac{\rho^*_{\mathrm{obs}}/T_{\mathrm{g}} - \rho^*_{\mathrm{atm+sfc}}}{t_{\mathrm{d}}t_{\mathrm{u}} + S\left(\rho^*_{\mathrm{obs}}/T_{\mathrm{g}} - \rho^*_{\mathrm{atm+sfc}}\right)}, \quad (1)$$

where $\rho^*_{\mathrm{obs}} = \pi L_v/\mu_{\mathrm{s}}E_s$ is the sensor reflectance expressed by the TOA (top of atmosphere) solar irradiance, E_s, and by the cosine of the solar zenith angle, $\mu_{\mathrm{s}} = cos(\theta_{\mathrm{s}})$. The other variables of Eq. (1), T_{g}, $\rho^*_{\mathrm{atm+sfc}}$, t_{S}, S, $t_{\mathrm{d,u}}$, are radiative quantities simulated with a spectral sampling of 2.5 nm covering the domain from 400 to 900 nm using the 6SV code. T_{g} is the gas transmittance; $\rho^*_{\mathrm{atm+sfc}}$ is composed by the atmospheric reflectance, called path radiance, by the roughened sea surface and by the whitecap; S is the atmospheric spherical albedo, (Kokhanovsky, 2008); and $t_{\mathrm{d,u}}$ are the downward and upward components of the total atmospheric transmittance (Vermote et al., 1997a, b).

The HICO@CRI algorithm computes the convolution of the radiative quantities, simulated with 2.5 nm spectral sampling, on the spectral response of the HICO™ sensor which is assumed to be assumed gaussian with the central wavelength and the FWHM provided in the header file of the image (i.e. 10 nm for the first 60 channels from 404 to 742 and 20 nm for the remaining 27 between 748 and 897 nm). The procedure is described in Bassani et al. (2010).

The atmospheric correction algorithms developed for the remote retrieval of ocean properties are usually based on the assumption of a negligible physical contribution of the target environment (IOCCG, 2010). The water near the coast instead could be influenced by the land surface characterized with high spectral albedo (Zibordi et al., 2009a). Thus using HICO@CRI, the water-leaving reflectance, ρ_{w}, is retrieved, removing the effect of the neighbouring pixels on the pixel viewed by the sensor, using the empirical formula employed in atmospheric correction algorithms (Bassani et al., 2012, 2010; Vermote et al., 1997b)

$$\rho_{\mathrm{w}} = \rho'_{\mathrm{w}} + \frac{t_{\mathrm{u}}^{\mathrm{dif}}}{t_{\mathrm{u}}^{\mathrm{dir}}}\left[\rho'_{\mathrm{w}} - < \rho'_{\mathrm{w}} >\right], \quad (2)$$

where $t_{\mathrm{u}}^{\mathrm{dir}}$ and $t_{\mathrm{u}}^{\mathrm{dif}}$ are the direct and diffuse components of the upward transmittance. In Eq. (2) $< \rho'_{\mathrm{w}} >$ is the mean of the pixels adjacent to the viewed pixel covering the swath of the HICO™ sensor, which is approximately 30 km^2.

The geolocated and geometric inputs required for HICO@CRI runs are loaded in the HICO@CRI algorithm from a file supplied with each HICO™ image, where the following data are contained: longitude (degrees), latitude (degrees), the viewing zenith (VZA) and azimuth (VAA) angles, and the solar zenith (SZA) and azimuth (SAA) angles, referring to each pixel of the image. These values permit to simulate the radiative quantities for each pixel by avoiding errors in calculating the geometrical configuration of the acquisition.

Concerning the atmospheric input, the HICO@CRI algorithm loads aerosol and gas parameters. Evaluation of the impact of the size distribution and refractive index of the aerosol on the results of the atmospheric correction over coastal areas needs an accurate aerosol loading, by the τ_{550} (Kaufman et al., 1997), and the columnar content of the gas with the absorption bands falling into sensor channels. At present, the gas parameters considered are the columnar content of water vapour, wvcc, and ozone, occ. The known and constrained properties related to the gas and to the aerosol loading guarantee that variability in the atmospheric correction results is only due to the microphysical properties of the aerosol. As regards the aerosol type, AERONET inversion products (i.e. the microphysical properties of the aerosol) or standard aerosol types (i.e. percentage of the basic components) can be introduced into the algorithm. The microphysical properties, downloaded from the AAOT station and used as input in the HICO@CRI, are the size distribution and the refractive index (cf. Fig. 2). Otherwise, in the developed algorithm, aerosol types can be introduced from the 6SV default types defined by the optical properties (Vermote et al., 2006), described in Sect. 3.

5 Results

The HICO™ images, reported in Table 1, were processed by applying the HICO@CRI algorithm. The geolocated and geometric inputs were taken from the ancillary data. The atmospheric inputs (τ_{550}, wvcc, and occ) were constrained by the AERONET products, while the parameters defining the type of aerosol were varied. In the first step, the the HICO@CRI algorithm results obtained considering the local microphysical properties of the aerosol as provided by the AAOT site at the HICO™ acquisition time were validated using in situ data. In the second step, the influence of the aerosol on the accuracy of the results of the atmospheric correction

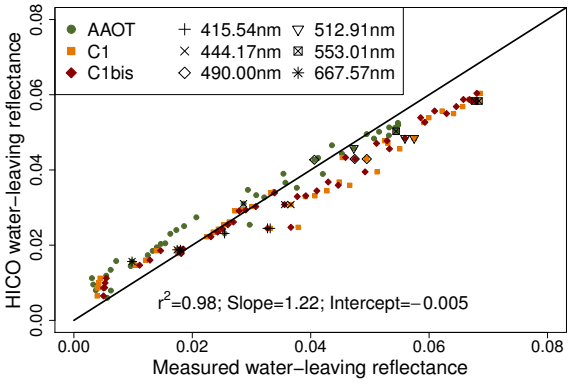

Figure 4. HICO™-derived $\rho_w(\lambda)$ versus in situ $\rho_w(\lambda)$ water-leaving reflectances at the three stations (AAOT, C1, C1bis) selected for the match-up (25 April 2013, Table 1). HICO™ $\rho_w(\lambda)$ was corrected with HICO@CRI using AERONET inversion products. The coloured symbols indicate the $\rho_w(\lambda)$ at the HICO™ channels in the 400–800 nm spectral range. The black symbols indicate the $\rho_w(\lambda)$ at the six wavelengths used for ocean colour studies. The black line represents the 1 : 1 line.

was performed comparing the water-leaving reflectance obtained considering optical properties of the three 6SV standard aerosol types (continental, maritime, and urban) and the reflectance obtained considering locally observed aerosol.

5.1 Validation of HICO@CRI algorithm

The water-leaving reflectance obtained from HICO™ images (12 May 2012 and 25 April 2013, Table 1), using HICO@CRI with AAOT aerosol inversion products, size distribution, and refractive index, were validated using in situ data. A time difference of 2 h between the satellite overpass and the in situ measurement reduced the number of match-up pairs. However this ensures that in situ measurements and HICO-derived ρ_w actually correspond, particularly considering the high spatial and temporal variability of coastal waters (Goyens et al., 2013). For each match-up pair, the ρ_w in situ measurement was resampled to HICO™ wavelengths and the median of the HICO™-derived $\rho_w(\lambda)$ was calculated over a 3 by 3 pixel window around the station (Goyens et al., 2013; Jamet et al., 2011).

Figure 4 shows the water-leaving reflectance obtained from HICO@CRI versus the in situ measurements overall the atmospheric window of the HICO™ spectral domain highlighting the wavelengths with black symbols used for ocean colour studies (Zibordi et al., 2009b). The high correlation index for the match-up sets ($r^2 = 0.98$) ensures a high accuracy of the water-leaving reflectance obtained from the atmospheric correction with the actual microphysical properties (size distribution and refractive index) of the aerosol. The regression parameters show similar values in the three stations with a slope close to the unit and the intercept negligible respect the values of water-leaving reflectance. Consequently, HICO@CRI with locally observed aerosol provides an accurate water-leaving reflectance across numerous discrete narrow bands. This thus forms a contiguous spectrum that permits the detection and identification of key biophysical properties of the water column and bottom capturing fine spectral absorption features not possible with multispectral sensors (Gitelson et al., 2011).

5.2 Standard aerosol types in HICO@CRI

The accuracy assessment of the water-leaving reflectance retrieved by HICO@CRI with standard aerosol types was performed with respect to the water-leaving reflectance retrieved by the local microphysical properties of the aerosol as measured by the AAOT site.

Three regions of interest (ROIs) were selected on the basis of the variability and representativity of the water surface relative to each HICO™ image (cf. Table 1). The difference between the radiance recorded by the sensor channels in correspondence of the channels close to the maximum, 553.0 nm, and the minimum, 684.8 nm, of the solar radiation was used. The radiance measured by the sensor was considered to classify the water surface separately from the atmospheric correction procedure. Figure 5 shows the ROIs, containing 2500 pixels, chosen for each HICO™ image used in this study. The red ROI (ROIrL) is representative of water with low luminosity in the image, the blue and green ROIs represent water with medium (ROIbM), and high (ROIgH) luminosity, respectively. The locations of the ROIs were defined with similar geometrical configurations in order to neglect radiative contribution on the sensor radiance, due to the viewing and illumination angles between the ROIs of each image. The ROIs were also selected close to the AAOT station in order to avoid the impact of horizontal atmospheric variability within the HICO™ scenes.

For each corrected image by the HICO@CRI algorithm, four mean reflectance values were calculated with respect to the three ROIs obtained for the three 6SV standard aerosol types and for the AERONET inversion products.

Figure 6 shows the average water-leaving reflectance retrieved using the AERONET inversion products calculated for each ROI (cf. Fig. 5) and used as a benchmark for the assessing of the radiative impact of the aerosol type on the atmospheric correction processing. The retrieval of the water-leaving reflectance was performed for high (ROIgH), medium (ROIbM), and low (ROIrL) reflectance of the water. The noisy reflectance can be attributed to the effect of the signal-to-noise (SNR) ratio of the HICO™ sensor calculated for low reflectance cases, as reported by Moses et al. (2012). The negative reflectance values obtained from correction of the HICO™ image acquired on 12 May 2012 are explained by the limits of accuracy in the radiative transfer simulation for the early morning irradiance case, as shown in Table 1. In addition, the negative reflectance values on 4 May 2011 are likely due to the loss of accuracy of the simulation

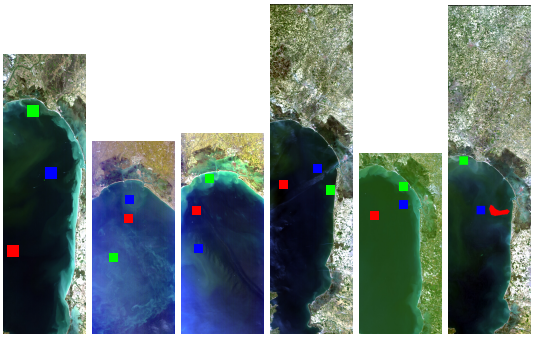

Figure 5. The available HICO™ images (using channel 11, 462 nm, for blue; 26, 548 nm, for green; 43, 645 nm, for red) show the three regions of interest (ROIs) chosen to evaluate the contribution of the aerosol types over different kind of water in the six available HICO™ images. The red is for the low, the blue for the medium and the green for the high luminosity of the water body.

results produced by the tri-modal size distribution obtained from CIMEL measurements, as shown in Fig. 2.

The metric for the accuracy assessment is based on the euclidean distance (ED), which is sensitive to the magnitude of the water-leaving reflectance (Shanmugam and SrinivasaPerumal, 2014) for each HICO™ channel with central wavelength λ_i.

$$\mathrm{ED}(\lambda_i) = \rho_w^{\mathrm{type}}(\lambda_i) - \rho_w^{\mathrm{phys}}(\lambda_i), \tag{3}$$

where $\rho_w^{\mathrm{type}}(\lambda_i)$ is the retrieved water-leaving reflectance by HICO@CRI algorithm with the continental, maritime and urban aerosol types; $\rho_w^{\mathrm{phys}}(\lambda_i)$ with the local microphysical properties of the aerosol as measured by the AAOT site.

In Fig. 7, $\mathrm{ED}(\lambda_i)$ is reported for the HICO™ channels centred in the atmospheric windows, in order to highlight the aerosol radiative impact thus avoiding the gas influence during the extinction modelling. Panels on the left show the $\mathrm{ED}(\lambda_i)$ for the image with the minimum available aerosol loading, $\tau_{550} = 0.01$, and panels on the right show the results for the maximum, $\tau_{550} = 0.27$. The ED highlights that in high aerosol loading conditions ($\tau_{550} = 0.27$), the distance between $\rho_w^{\mathrm{type}}(\lambda_i)$ and $\rho_w^{\mathrm{phys}}(\lambda_i)$ is more evident than in low aerosol loading conditions ($\tau_{550} = 0.01$) over the sensor spectral domain if a standard aerosol type is used rather than the locally observed aerosol.

The root mean square error (RMSE) was normalized to the distance between the outer limits (maximum and minimum) of each retrieved water-leaving reflectance. The values of the normalized RMSE (NRMSE) were calculated in order to assess the accuracy of the retrieved water leaving reflectance by each 6SV standard aerosol type with respect to the measured aerosol.

$$\mathrm{NRMSE} = \frac{\sum_i \mathrm{ED}(\lambda_i)}{\max[\rho_w^{\mathrm{phys}}(\lambda_i)] - \min[\rho_w^{\mathrm{phys}}(\lambda_i)]} \tag{4}$$

To complete the evaluation of the hyperspectral similarity between the water-leaving reflectance obtained from HICO@CRI with standard types and locally observed aerosol, the metric introduced in Granahan and Sweet (2001) was considered. The difference between two hyperspectral vectors is expressed by d_e taking into account the brightness of the two spectra and $\hat{r}^2$ accounting for the spectral behaviour (Granahan and Sweet, 2001)

$$d_e = \sqrt{\frac{1}{N_c}\sum_{i=1}^{N_c}(\mathrm{ED}(\lambda_i))^2}, \tag{5}$$

$$\hat{r}^2 = 1 - r^2, \tag{6}$$

where N_c are the HICO™ channels into atmospheric window. The spectral similarity value (SSV, $\mathrm{SSV} \in [0, \sqrt{2}]$) evaluates the similarity of both the brightness and spectral behaviour of the retrieved hyperspectral reflectance with standard and observed aerosol (Shanmugam and SrinivasaPerumal, 2014; Granahan and Sweet, 2001).

$$\mathrm{SSV} = \sqrt{d_e^2 + \hat{r}^2} \tag{7}$$

Figure 8 shows the NRMSE and SSV vs. the τ_{550} for the three ROIs, where the water-leaving reflectance accuracy decreases with growing aerosol loading, particularly when an unsuitable aerosol type is selected. The aerosol loading slowly changes the accuracy of the atmospheric correction results if an aerosol type, with similar optical properties as the AERONET inversion products, is considered (Fig. 3). In the case study, the continental aerosol best satisfies this condition, whereas the accuracy decreases more rapidly if the urban aerosol is selected.

During acquisition periods, aerosol was mainly distributed in the fine mode, showing a non negligible imaginary part of the refractive index, with the exception of 4 May 2011 and 25 April 2013. The NRMSE and the SSV for the 4 May 2011 were higher than the other ones (Fig. 8). The imaginary part of the refractive index is only negligible for the aerosol type during the HICO™ acquisition of 4 May 2011, as shown in Fig. 2. Thus, the results show that the radiative impact of aerosol absorption plays a crucial role in the atmospheric correction of hyperspectral data over water target in coastal environment as reported in IOCCG (2010) for multispectral data. On the other hand, Fig. 2 shows a size distribution of 25 April 2013 with a predominance in coarse mode. The aerosol size weakly affects the accuracy of the retrieved water-leaving reflectance, as shown in Fig. 8 in the case study of 25 April 2013 defined with a high aerosol loading, $\tau_{550} = 0.27$.

Results of these case studies highlight how the water-leaving reflectance accuracy decreases for a higher aerosol loading, particularly when the atmospheric correction is performed by the HICO@CRI algorithm using the aerosol standard type which does not represent the local aerosol. The

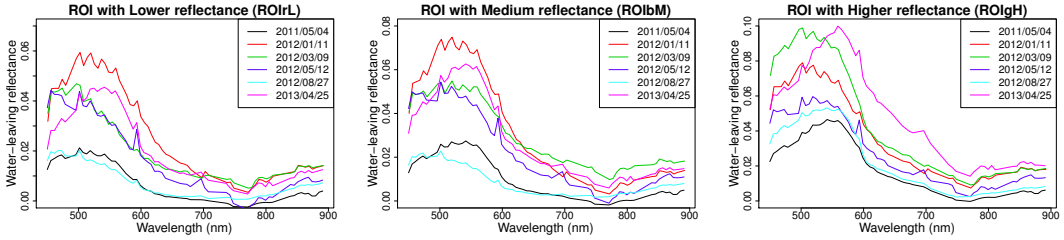

Figure 6. The mean water-leaving reflectance calculated in the ROIs (ROIrL, ROIbM, ROIgH) of the HICO™ images, applying HICO@CRI algorithm with the AERONET inversion products provided by AAOT station.

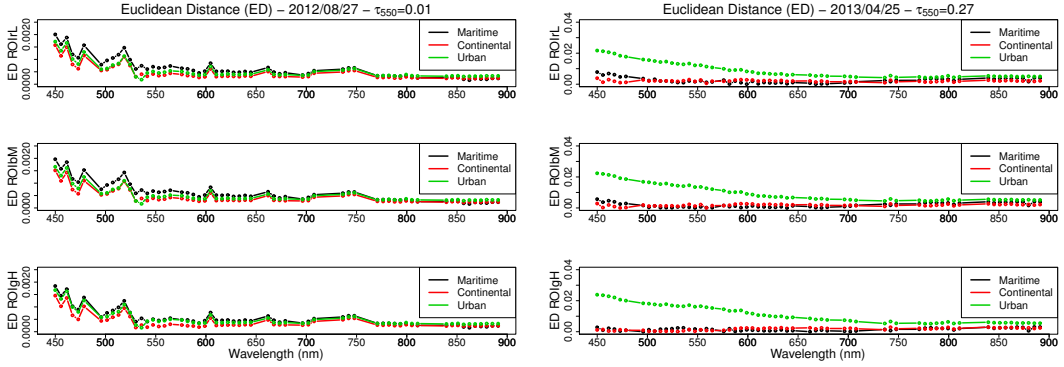

Figure 7. The euclidean distance (ED(λ_i)) between the mean water-leaving reflectance calculated in the ROIs (ROIrL, ROIbM, ROIgH) with the standard aerosol types (maritime, continental and urban) and the CIMEL inversion products. On the right, the ED(λ_i) calculated for the HICO image acquired the 27 August 2012 with $\tau_{550} = 0.01$, and on the left, the image acquired the 25 April 2013 with $\tau_{550} = 0.27$.

water-leaving reflectance obtained using the AERONET inversion products is mainly correlated to the reflectance obtained using the continental aerosol type, independently from the luminosity of the ROIs, as highlighted in Fig. 8. This is also observed for 4 May 2011, although the water-leaving reflectance obtained from the HICO@CRI with AERONET inversion products for the ROIrL shows very low values. In addition, the tri-modal size distribution observed on 4 May 2011 could be related to the spike shown in Fig. 8 for $\tau_{550} = 0.08$. This result suggests that the sensitivity of the 6SV to a tri-modal size distribution needs to be investigated in more depth when an atmospheric correction of hyperspectral data over water surface is performed.

6 Discussion and conclusions

This study has highlighted the impact of the microphysical properties of aerosol (i.e. size distribution and refractive index) on the accuracy of the results of the physically based atmospheric correction of hyperspectral data acquired over coastal water with clear improvement on the simplification typical of the aerosol standard types (Zibordi et al., 2009a; Gordon and Wang, 1994). The HICO@CRI (HICO™ ATmospherically Corrected Reflectance Image) atmospheric correction algorithm was developed and applied to HICO™ images acquired in the northern Mediterranean basin, when inversion products of the AAOT (Acqua Alta Oceanographic Tower) site were available. The analysis was performed for the HICO™ images acquired for different values of the aerosol loading ($\tau_{550} < 0.3$) and with clear-sky conditions. The results obtained from the HICO@CRI algorithm using the local microphysical properties of the aerosol were validated with in situ measurements available from oceanographic campaigns. These results using the local measured aerosol were used as a benchmark to evaluate the accuracy of the hyperspectral water-leaving reflectance, ρ_w, obtained from the atmospheric correction performed using the 6SV standard aerosol types. Results show that the accuracy of the retrieved water-leaving reflectance depends on the aerosol microphysical properties used in the atmospheric correction processing, as well as on the influence of the aerosol loading.

The NRMSE and the SSV were chosen to perform the accuracy assessment of the water-leaving reflectance obtained by atmospheric correction with aerosol standard type with respect to the AAOT aerosol microphysical properties. The NRMSE and SSV quantify the decrease in the accuracy of the retrieved ρ_w with increasing aerosol loading if standard aerosol types are used instead of the local observed aerosol (Fig. 8). In the case study, the results suggest that the local observed aerosol during the HICO™ acquisition times is always better represented by continental type, maintaining a high accuracy as highlighted by the low value of the

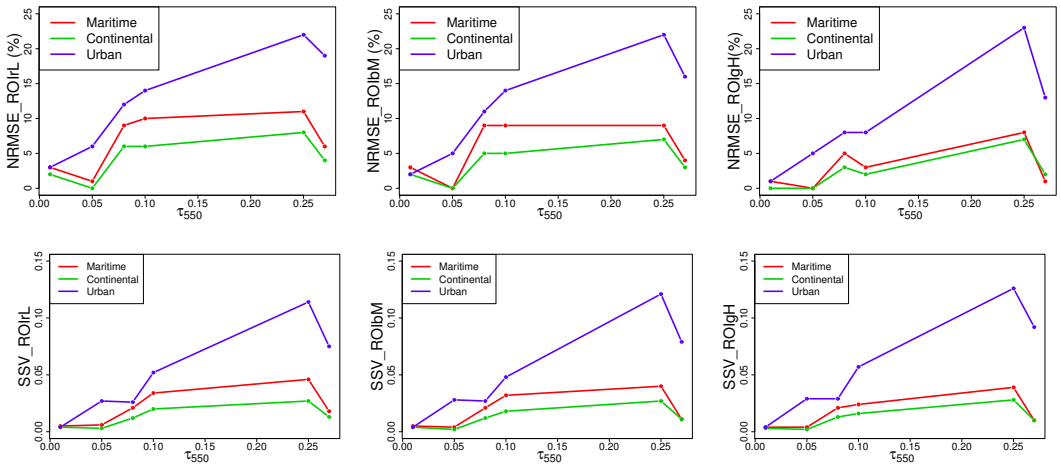

Figure 8. The NRMSE and SSV of the water-leaving reflectance retrieved with the aerosol types (urban, continental, and maritime) with respect to the AERONET inversion products, calculated for the ROIs. Starting from the left, the calculation for the low, medium and high reflectance water types.

SSV and NRMSE with an increased aerosol loading (Fig. 8). The increased aerosol loading decreases the ρ_w accuracy except in coarse mode predominance (25 April 2013 in Fig. 2). This is when the accuracy seems to be slightly affected by the aerosol type, probably as a results of the lower effect of size distribution compared to the refractive index effect on the simulation of the radiative field. The lowest accuracy values were obtained with the urban aerosol because the radiative quantities in Eqs. (1) and (2) depend on the higher contribution of the absorption of this aerosol type, as also widely demonstrated for multispectral data (IOCCG, 2010). This situation is confirmed by the optical properties of the urban aerosol presented in Fig. 3.

Finally, the NRMSE and SSV quantify how the choice of an unsuitable standard aerosol type affects the hyperspectral water-leaving reflectance over this study area following up the limit detected by Zibordi et al. (2006, 2009a) of standard aerosol types to well represent the local microphysical properties.

We believe that the results of this work are useful for applying atmospheric correction algorithms to hyperspectral remote sensing data when used in water quality applications in coastal environments. Indeed, the highest possible accuracy of the hyperspectral water-leaving reflectance improves the detection capability of the dedicated algorithms for the retrieval of water quality parameters (Chlorophyll, Total Suspended Matter and Colored Dissolved Organic Matter) (Gitelson et al., 2011; Lee et al., 2007; Zibordi et al., 2011; Giardino et al., 2010; Guanter et al., 2010; Brando and Dekker, 2003). For example, if the chl *a* concentration is estimated according to band-ratio, which makes use of a red (680 nm) to very near-infrared (700 nm) wavelengths, the advantage of having a signal on a contiguous spectrum relies on the possibility of defining the algorithm according to the shift of the near-infrared reflectance band to be used (Schalles, 2006). In case of spectral inversion procedures, a hyperspectral data set can facilitate a physics-based modelling approach to quantitatively retrieve multiple constituents of interest (e.g. SPM (suspended particulate matter), CDOM (coloured dissolved organic matter), and phytoplankton functional types) (Devred et al. (2013) and references therein). Overall, hyperspectral remote sensing provides essential data to de-convolve the remotely sensed signal and, thence, to detect the water components that could be missed by multispectral instruments.

Acknowledgements. This work was undertaken as part of the CLAM-PHYM Project, funded by the Italian Space Agency (ASI, contract No. I/015/11/0). We are grateful to G. Zibordi for his valuable comments and for providing data on the AAOT station belonging to the AERONET and AERONET-OC networks. The HICO™ images used for this study were provided by the Naval Research Laboratory, USA and the Oregon State University within the project "Using HICO™ data for the preparation of the incoming Italian satellite hyperspectral mission PRISMA". Thanks are also due to A. Pietrodangelo and to S. Schmidt for their support revising this manuscript.

Edited by: S. Schmidt

References

Ahmad, Z., Franz, B. A., McClain, C. R., Kwiatkowska, E. J., Werdell, J., Shettle, E. P., and Holben, B. N.: New aerosol models for the retrieval of aerosol optical thickness and normalized water-leaving radiances from the SeaWiFS and MODIS sensors over coastal regions and open oceans, Appl. Opt., 49, 5545–5560, doi:10.1364/AO.49.005545, 2010.

Amin, R., Lewis, D., Gould, R., Hou, W., Lawson, A., Ondrusek, M., and Arnone, R.: Assessing the Application of Cloud-Shadow

Atmospheric Correction Algorithm on HICO, IEEE T. Geosci. Remote, 52, 2646–2653, doi:10.1109/TGRS.2013.2264166, 2014.

Antoine, D. and Morel, A.: A multiple scattering algorithm for atmospheric correction of remotely sensed ocean colour (MERIS instrument): principle and implementation for atmospheres carrying various aerosols including absorbing ones, Int. J. Remote Sens., 20, 1875–1916, doi:10.1080/014311699212533, 1999.

Arabas, S., Schellens, M., Coulais, A., Gales, J., and Messmer, P.: GNU Data Language (GDL) – a free and open-source implementation of IDL, in: Geophysical Research Abstracts, vol. 12 of EGU General Assembly 2010, pp. EGU2010–924–1, Vienna, Austria, 2010.

Bassani, C., Cavalli, R. M., and Pignatti, S.: Aerosol optical retrieval and surface reflectance from airborne remote sensing data over land, Sensors, 10, 6421–6438, doi:10.3390/s100706421, 2010.

Bassani, C., Cavalli, R. M., and Antonelli, P.: Influence of aerosol and surface reflectance variability on hyperspectral observed radiance, Atmos. Meas. Tech., 5, 1193–1203, doi:10.5194/amt-5-1193-2012, 2012.

Braga, F., Giardino, C., Bassani, C., Matta, E., Candiani, G., Strömbeck, N., Adamo, M., and Bresciani, M.: Assessing water quality in the northern Adriatic Sea from HICO data, Remote Sensing Letters, 4, 1028–1037, doi:10.1080/2150704X.2013.830203, 2013.

Brando, V. and Dekker, A.: Satellite hyperspectral remote sensing for estimating estuarine and coastal water quality, Geoscience and Remote Sensing, IEEE T. Geosci. Remote, 41, 1378–1387, doi:10.1109/TGRS.2003.812907, 2003.

Coulais, A., Schellens, M., Gales, J., Arabas, S., Boquien, M., Chanial, P., Messmer, P., and Fillmore, D.: Status of GDL-GNU Data Language, in: Astronomical Data Analysis Software and Systems XIX, vol. 434 of ASP Conference Series, Springer, Sapporo, Japan, 2009.

d'Almeida, G. A., Koepke, P., and Shettle, E. P.: Atmospheric aerosols: global climatology and radiative characteristics, A. DEEPAK Publishing, Hampton, Virginia, USA, 1991.

Devred, E., Turpie, K. R., Moses, W., Klemas, V. V., Moisan, T., Babin, M., Toro-Farmer, G., Forget, M.-H., and Jo, Y.-H.: Future Retrievals of Water Column Bio-Optical Properties using the Hyperspectral Infrared Imager (HyspIRI), Remote Sensing, 5, 6812–6837, doi:10.3390/rs5126812, 2013.

Gao, B.-C., Montes, M. J., Ahmad, Z., and Davis, C. O.: Atmospheric correction algorithm for hyperspectral remote sensing of ocean color from space, Appl. Opt., 39, 887–896, doi:10.1364/AO.39.000887, 2000.

Gao, B.-C., Montes, M. J., Davis, C. O., and Goetz, A. F. H.: Atmospheric correction algorithms for hyperspectral remote sensing data of land and ocean, Remote Sens. Environ., 113, 17–24, doi:10.1016/j.rse.2007.12.015, 2009.

Gao, B.-C., Li, R.-R., Lucke, R. L., Davis, C. O., Bevilacqua, R. M., Korwan, D. R., Montes, M. J., Bowles, J. H., and Corson, M. R.: Vicarious calibrations of HICO data acquired from the International Space Station, Appl. Optics, 51, 2559–2567, doi:10.1364/AO.51.002559, 2012.

Giardino, C., Bresciani, M., Pilkaitytė, R., Bartoli, M., and Razinkovas, A.: In situ measurements and satellite remote sensing of case 2 waters: first results from the Curonian Lagoon, Oceanologia, 52, 197–210, doi:10.5697/oc.52-2.197, 2010.

Gitelson, A. A., Gao, B.-C., Li, R.-R., Berdnikov, S., and Saprygin, V.: Estimation of chlorophyll-a concentration in productive turbid waters using a Hyperspectral Imager for the Coastal Ocean – the Azov Sea case study, Environ. Res. Lett., 6, 024023, doi:10.1088/1748-9326/6/2/024023, 2011.

Gordon, H. R. and Wang, M.: Surface-roughness considerations for atmospheric correction of ocean color sensors. II: Error in the retrieved water-leaving radiance, Appl. Opt., 31, 4261–4267, doi:10.1364/AO.31.004261, 1992.

Gordon, H. R. and Wang, M.: Retrieval of water-leaving radiance and aerosol optical thickness over the oceans with SeaWiFS: a preliminary algorithm, Appl. Opt., 33, 443–452, doi:10.1364/AO.33.000443, 1994.

Goyens, C., Jamet, C., and Schroeder, T.: Evaluation of four atmospheric correction algorithms for MODIS-Aqua images over contrasted coastal waters, Remote Sens. Environ., 131, 63–75, doi:10.1016/j.rse.2012.12.006, 2013.

Granahan, J. and Sweet, J.: An Evaluation Of Atmospheric Correction Techniques Using The Spectral Similarity Scale, in: Proceedings of the IEEE 2001 International Geoscience and Remote Sensing Symposium, 5, 2022–2024, 2001.

Guanter, L., Ruiz-Verdú, A., Odermatt, D., Giardino, C., Simis, S., Estellés, V., Heege, T., Domínguez-Gómez, J. A., and Moreno, J.: Atmospheric correction of ENVISAT/MERIS data over inland waters: Validation for European lakes, Remote Sens. Environ., 114, 467–480, doi:10.1016/j.rse.2009.10.004, 2010.

Holben, B., Eck, T., Slutsker, I., Tanré, D., Buis, J., Setzer, A., Vermote, E., Reagan, J., Kaufman, Y., Nakajima, T., Lavenu, F., Jankowiak, I., and Smirnov, A.: AERONET – A Federated Instrument Network and Data Archive for Aerosol Characterization, Remote Sens. Environ., 66, 1–16, doi:10.1016/S0034-4257(98)00031-5, 1998.

Hommersom, A., Kratzer, S., Laanen, M., Ansko, I., Ligi, M., Bresciani, M., Giardino, C., Beltrán-Abaunza, J. M., Moore, G., Wernand, M., and Peters, S.: Intercomparison in the field between the new WISP-3 and other radiometers (TriOS Ramses, ASD FieldSpec, and TACCS), J. Appl. Remote Sens., 6, 063615–063615, doi:10.1117/1.JRS.6.063615, 2012.

IOCCG: Atmospheric Correction for Remotely-Sensed Ocean-Colour Products, in: Reports and Monographs of the International Ocean-Colour Coordinating Group, edited by: Wang, M., vol. No. 10 of Reports of the International Ocean Colour Coordinating Group, IOCCG, Dartmouth, Canada, http://www.ioccg.org/reports/report10.pdf, 2010.

Jamet, C., Loisel, H., Kuchinke, C. P., Ruddick, K., Zibordi, G., and Feng, H.: Comparison of three SeaWiFS atmospheric correction algorithms for turbid waters using AERONET-OC measurements, Remote Sens. Environ., 115, 1955–1965, doi:10.1016/j.rse.2011.03.018, 2011.

Kaufman, Y. J., Tanré, D., Remer, L. A., Vermote, E. F., Chu, A., and Holben, B. N.: Operational remote sensing of tropospheric aerosol over land from EOS moderate resolution imaging spectroradiometer, J. Geophys. Res., 102, 17051–17067, doi:10.1029/96JD03988, 1997.

Kokhanovsky, A. A.: Aerosol optics: light absorption and scattering by particles in the atmosphere, Praxis Publishing Ltd, Chichester, UK, 2008.

Kotchenova, S. Y. and Vermote, E. F.: Validation of a vector version of the 6S radiative transfer code for atmospheric correction of satellite data. Part II. Homogeneous Lambertian and anisotropic surface, Appl. Optics, 46, 4455–4464, doi:10.1364/AO.46.004455, 2007.

Kotchenova, S. Y., Vermote, E. F., Matarrese, R., and Frank J. Klemm, J.: Validation of a vector version of the 6S radiative transfer code for atmospheric correction of satellite data. Part I: Path radiance, Appl. Optics, 45, 6762–6774, doi:10.1364/AO.45.006762, 2006.

Kotchenova, S. Y., Vermote, E. F., Levy, R., and Lyapustin, A.: Radiative transfer codes for atmospheric correction and aerosol retrieval: Intercomparison study, Appl. Optics, 47, 2215–2226, doi:10.1364/AO.47.002215, 2008.

Lee, Z., Casey, B., Arnone, R., Weidemann, A., Parsons, R., Montes, M. J., Gao, B.-C., Goode, W., Davis, C., and Dye, J.: Water and bottom properties of a coastal environment derived from Hyperion data measured from the EO-1 spacecraft platform, J. Appl. Remote Sens., 1, 011502, doi:10.1117/1.2822610, 2007.

Lenoble, J.: Radiative Transfer in scattering and absorbing atmospheres: standard computational procedures, A. DEEPAK Publishing, Hampton, Virginia, USA, 1985.

Lucke, R. L., Corson, M., McGlothlin, N. R., Butcher, S. D., Wood, D. L., Korwan, D. R., Li, R. R., Snyder, W. A., Davis, C. O., and Chen, D. T.: Hyperspectral Imager for the Coastal Ocean: instrument description and first images, Appl. Optics, 50, 1501–1516, doi:10.1364/AO.50.001501, 2011.

McClain, C. R.: A decade of satellite ocean color observations, Annual Review of Marine Science, 1, 19–42, doi:10.1146/annurev.marine.010908.163650, 2009.

Mélin, F., Clerici, M., Zibordi, G., and Bulgarelli, B.: Aerosol variability in the Adriatic Sea from automated optical field measurements and Sea-viewing Wide Fiel-of-view Sensor (SeaWiFS), J. Geophys. Res., 111, D22201, doi:10.1029/2006JD007226, 2006.

Mélin, F., Zibordi, G., and Berthon, J.-F.: Assessment of satellite ocean color products at a coastal site, Remote Sens. Environ., 110, 192–215, doi:10.1016/j.rse.2007.02.026, 2007.

Morel, A. and Gentili, G.: Diffuse reflectance of oceanic waters: its dependence on Sun angle as influenced by the molecular scattering contribution, Appl. Optics, 30, 4427–4438, doi:10.1364/AO.30.004427, 1991.

Morel, A. and Gentili, G.: Diffuse reflectance of oceanic waters. III. Implication of bidirectionality for the remote-sensing problem, Applied Optics, 35, 4850–4862, doi:10.1364/AO.35.004850, 1996.

Moses, W. J., Bowles, J. H., Lucke, R. L., and Corson, M. R.: Impact of signal-to-noise ratio in a hyperspectral sensor on the accuracy of biophysical parameter estimation in case II waters, Optics Express, 20, 4309–4330, doi:10.1364/OE.20.004309, 2012.

Schalles, J. F.: Optical remote sensing techniques to estimate phytoplankton chlorophyll a concentrations in coastal, in: Remote sensing of aquatic coastal ecosystem processes, edited by: Richardson, L. L. and LeDrew, E. F., vol. 9 of Remote Sensing and Digital Image Processing, Springer, the Netherlands, 27–79, doi:10.1007/1-4020-3968-9_3, 2006.

Shanmugam, S. and SrinivasaPerumal, P.: Spectral matching approaches in hyperspectral image processing, Int. J. Remote Sens., 35, 8217–8251, doi:10.1080/01431161.2014.980922, 2014.

Smirnov, A., Holben, B. N., Giles, D. M., Slutsker, I., O'Neill, N. T., Eck, T. F., Macke, A., Croot, P., Courcoux, Y., Sakerin, S. M., Smyth, T. J., Zielinski, T., Zibordi, G., Goes, J. I., Harvey, M. J., Quinn, P. K., Nelson, N. B., Radionov, V. F., Duarte, C. M., Losno, R., Sciare, J., Voss, K. J., Kinne, S., Nalli, N. R., Joseph, E., Krishna Moorthy, K., Covert, D. S., Gulev, S. K., Milinevsky, G., Larouche, P., Belanger, S., Horne, E., Chin, M., Remer, L. A., Kahn, R. A., Reid, J. S., Schulz, M., Heald, C. L., Zhang, J., Lapina, K., Kleidman, R. G., Griesfeller, J., Gaitley, B. J., Tan, Q., and Diehl, T. L.: Maritime aerosol network as a component of AERONET – first results and comparison with global aerosol models and satellite retrievals, Atmos. Meas. Tech., 4, 583–597, doi:10.5194/amt-4-583-2011, 2011.

Tanré, D., Kaufman, Y. J., Herman, M., and Mattoo, S.: Remote sensing of aerosol properties over oceans using the MODIS/EOS spectral radiances, J. Geophys. Res.-Atmos., 102, 16971–16988, doi:10.1029/96JD03437, 1997.

Vermote, E. F. and Kotchenova, S.: Atmospheric correction for the monitoring of land surfaces, J. Geophys. Res.-Atmos., 113, n/a–n/a, doi:10.1029/2007JD009662, 2008.

Vermote, E. F., Saleous, N. E., Justice, C., Kaufman, Y., Privette, J., Remer, L., Roger, J., and Tanré, D.: Atmospheric correction of visible to middle-infrared EOS-MODIS data over land surfaces: Background, operational algorithm and validation, J. Geophys. Res., 102, 675–686, doi:10.1029/97JD00201, 1997a.

Vermote, E. F., Tanré, D., Deuzé, J. L., Herman, M., and Morcrette, J. J.: Second simulation of the satellite signal in the solar spectrum, 6S: An overview, IEEE T. Geosci. Remote, 35, 675–686, doi:10.1109/36.581987, 1997b.

Vermote, E. F., Tanré, D., Deuzé, Herman, M., Morcrette, J. J., and Kotchenova, S. Y.: Second Simulation of a Satellite Signal in the Solar Spectrum – Vector (6SV), http://6s.ltdri.org, 6S User Guide Version 3, 2006.

Zibordi, G., Mélin, F., and Berthon, J.-F.: Comparison of SeaWiFS, MODIS and MERIS radiometric products at a coastal site, Geophys. Res. Lett., 33, L06617, doi:10.1029/2006GL025778, 2006.

Zibordi, G., Berthon, J.-F., Mélin, F., D'Alimonte, D., and Kaitala, S.: Validation of satellite ocean color primary products at optically complex coastal sites: Northern Adriatic Sea, Northern Baltic Proper and Gulf of Finland, Remote Sens. Environ., 113, 2574–2591, doi:10.1016/j.rse.2009.07.013, 2009a.

Zibordi, G., Mélin, F., Berthon, J.-F., Holben, B., Slutsker, I., Giles, D., D'Alimonte, D., Vandemark, D., Feng, H., Schuster, G., Fabbri, B. E., Kaitala, S., and Seppälä, J.: AERONET-OC: A network for the Validation of Ocean Color Primary Products, J. Atmos. Ocean Tech., 26, 1634–1651, doi:10.1175/2009JTECHO654.1, 2009b.

Zibordi, G., Berthon, J.-F., Mélin, F., and D'Alimonte, D.: Cross-site consistent in situ measurements for satellite ocean color applications: The BiOMaP radiometric dataset, Remote Sens. Environ., 115, 2104–2115, doi:10.1016/j.rse.2011.04.013, 2011.